Doubly resonant sub-ppt photoacoustic gas detection with eight decades dynamic range

Zhen Wang [a,b], Qiang Wang [a,c,*], Hui Zhang [a,c], Simone Borri [d], Iacopo Galli [d], Angelo Sampaolo [e], Pietro Patimisco [e], Vincenzo Luigi Spagnolo [e], Paolo De Natale [d], Wei Ren [b,**]

[a] State Key Laboratory of Applied Optics, Changchun Institute of Optics, Fine Mechanics and Physics, Chinese Academy of Sciences, Changchun 130033, China
[b] Department of Mechanical and Automation Engineering, The Chinese University of Hong Kong, New Territories, Hong Kong, China
[c] University of Chinese Academy of Sciences, Beijing 100049, China
[d] CNR-INO – Istituto Nazionale di Ottica, and LENS – European Laboratory for Nonlinear Spectroscopy, 50019 Sesto Fiorentino, Italy
[e] PolySense Lab – Dipartimento Interateneo di Fisica, University and Politecnico of Bari, Via Amendola 173, Bari, Italy

ABSTRACT

Photoacoustic spectroscopy (PAS) based gas sensors with high sensitivity, wide dynamic range, low cost, and small footprint are desirable in energy, environment, safety, and public health. However, most works have focused on either acoustic resonator to enhance acoustic wave or optical resonator to enhance optical wave. Herein, we develop a gas sensor based on doubly resonant PAS in which the acoustic and optical waves are simultaneously enhanced using combined optical and acoustic resonators in a centimeter-long configuration. Not only the lower detection limit is enhanced by the double standing waves, but also the upper detection limit is expanded due to the short resonators. As an example, we developed a sensor by detecting acetylene (C_2H_2), achieving a noise equivalent absorption of 5.7×10^{-13} cm^{-1} and a dynamic range of eight orders. Compared to the state-of-the-art PAS gas sensors, the developed sensor achieves a record sensitivity and dynamic range.

1. Introduction

Laser-based optical gas sensors are increasingly required in many fields such as environmental monitoring [1,2], marine science [3,4], biological studies [5,6], and breath analysis [7,8]. By measuring light attenuation through a gas sample, quantitative gas analysis can be performed. To enhance sensitivity, the absorption path length can be increased to hundreds of meters by a multipass cell or several kilometers by a high-finesse optical cavity. Among the most sensitive laser-based gas sensing techniques, noise-immune cavity-enhanced optical heterodyne molecular spectroscopy (NICE-OHMS) achieved 10^{-14} cm^{-1} in noise equivalent absorption (NEA) [9]. The minimum detectable concentration of a specific molecule has been achieved by saturated-absorption cavity ring-down (SCAR) with a limit of a few parts-per-quadrillion (ppq) [6,10]. However, the relatively long cavity used in this class of gas sensors sets a limit on the dynamic range because the high finesse degrades even at low gas concentrations, which also leads to, in turn, the large overall footprint and weight. For example,

with a cavity finesse of 30,000 and a cavity length of 37.8 cm used in NICE-OHMS, the dynamic range is limited to four orders of magnitude [11]. Dynamic range is a very important parameter of gas sensors. For example, the NH_3 concentration changes by orders from tens of parts-per-million (ppm) to parts-per-billion (ppb) in applications including chemical hazards monitoring for occupational safety and health, contaminant control in hydrogen source for fuel cell, and contaminant requirement in lithography processing in semiconductor industry [12].

To get a combined high sensitivity and wide dynamic range, photoacoustic spectroscopy (PAS) is a promising candidate as the acoustic signal linearly increases with laser power, rather than a long absorption path. Numerous studies have been focused on applying various acoustic transducers and designing resonators to enhance the acoustic wave [13–16]. An optical resonator can also be used to enhance the laser power by precisely matching the cavity mode and laser frequency using low-frequency dither locking [17,18], optical feedback [19,20], and Pound-Drever-Hall (PDH) locking method [21,22]. However, compared

---

to the well-assessed cavity ring-down spectroscopy (CRDS) and NICE-OHMS techniques (10^{-14}–10^{-13} cm^{-1} in NEA), the NEA of state-of-the-art PAS gas sensors is limited to 10^{-11}–10^{-8} cm^{-1}, while the dynamic range is limited to five orders of magnitude [13,14,17,21–24]. It is worth mentioning that researchers recently tried to combine an acoustic resonator with an optical resonator to advance the performance [25]. However, the sensitivity and dynamic range cannot be simultaneously improved because of the limited optical and acoustic buildup factors, noise floor limited by the optical feedback strategy and the long optical cavity with a Brewster window [25]. A high-efficiency doubly resonant strategy, which can enhance the intracavity PAS signal by orders linearly, is worth pursuing.

In this work, we report a PAS sensor with opto-acoustic resonance enhancement for gas detection with ultra-high sensitivity and ultra-wide dynamic range. The proposed photoacoustic design, leveraging on a double standing wave effect, achieves a combined acoustic amplification factor of 144 and laser power enhancement of almost three orders of magnitude. As a proof-of-principle, we show that our C_2H_2 sensor reaches a record sensitivity of 10^{-13} cm^{-1} (NEA) and a record dynamic range of eight orders of magnitude.

2. Working principle

Fig. 1 shows the basics of opto-acoustic resonance for PAS. The core gas sensing element consists of an optical resonator, an acoustic resonator, and an acoustic transducer, which are arranged in a coupled configuration. Indeed, when the optical frequency of the incident laser is in resonance with a longitudinal cavity mode of the optical resonator, a standing optical wave is formed between the resonator mirrors. A high-finesse optical resonator can significantly build up the laser power [26], by several orders of magnitude, directly enhancing the photoacoustic signal. The laser intensity is modulated at the same resonance frequency as the acoustic resonator and transducer. A specifically designed one-dimensional longitudinal tube can be used to amplify the acoustic signal by forming a standing acoustic wave inside it. Any types of acoustic transducers can be used to detect the amplified acoustic wave. In this work, we use a quartz tuning fork (QTF) with a high Q-factor for demonstration. The QTF locates nearby the antinode of the standing acoustic wave, which is generated by the acoustic resonator composed of two stainless-steel tubes placed at the opposite sides of the QTF [27].

The frequency-dependent photoacoustic signal (S) at its resonant frequency f is given by [28]:

$$S = b \times g \times K \times W_{in}(\lambda)\left(1 - e^{-\alpha_{eff}(\lambda)}\right)\varepsilon(f, \tau(P)) \tag{1}$$

where b is the laser power buildup factor, g is the acoustic wave enhancement factor, K is the sensor constant, W_{in} is the incident laser power, λ is the laser wavelength, $\alpha_{eff}(\lambda)$ is the effective absorbance by the analyte, $\tau(P)$ is the relaxation time at the gas pressure P, and ε is the radiation-to-sound conversion efficiency, which depends on f and τ. Note that the factor g is independent of laser power but is related to the
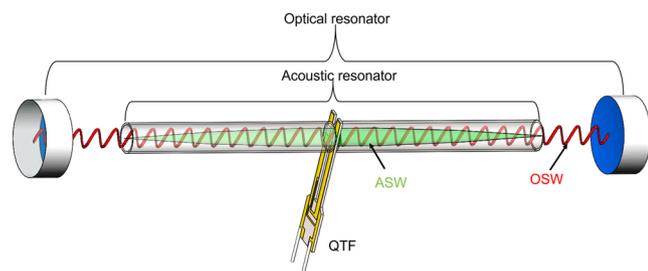
geometry, to the material, and to the Q-factor of the acoustic resonator, as well as to the frequency of acoustic waves [29]. The power buildup factor b is determined by coupling efficiency and finesse of the optical resonator which needs to be properly selected so that a wide dynamic range and a high sensitivity can be simultaneously obtained (Appendix A).

3. Experimental setup

The schematic of the doubly resonant PAS sensor is shown in Fig. 2. An external cavity diode laser (ECDL, TOPTICA Photonics) is used to detect the P(11) transition of C_2H_2 at 1531.59 nm. The ECDL is phase modulated by an electro-optic modulator (EOM, iXblue Photonics) at 20 MHz and locked to the optical resonator using the PDH method [30]. The polarization beam splitter is used with the quarter-wave plate to pick up the reflected beam from the optical resonator, which is then detected by a photodetector (PD1). Details of the application of the PDH method to PAS can be found in [21]. In this work, the current and piezo transducer (PZT) feedback loops of the ECDL are both used to improve the locking performance. Each mirror (Layertec Inc.) of the optical resonator has a radius of curvature of 150 mm and reflectivity of 99.923% (finesse 4078) at the laser wavelength, as measured by cavity ring-down (see Supplementary Note 1). Compared with other cavity-enhanced absorption spectroscopic methods [6,9], the optical resonator used here for the opto-acoustic resonance features a much shorter length (60 mm in this work). Two mode matching lenses (focus length: $L_1 =30$ mm and $L_2 =50$ mm) and a photodetector (PD2) are used to maximize the coupling efficiency (84%) between the laser and the optical resonator (see Supplementary Note 2). With a maximum incident laser power of 300 mW, the intracavity optical power is boosted to 264 W in this work (Appendix B).

The intracavity laser beam passes through the acoustic resonator, which consists of two stainless-steel tubes (inner diameter 1.3 mm, length 23 mm), and does not touch any surface. The central axis of the acoustic resonator is placed 1.2 mm below the top of the QTF prongs to optimize the piezoelectrical conversion efficiency [15]. The two tubes are placed at a distance of ~60 μm from the QTF, so that it lies near the antinode of the acoustic wave and leaves its Q-factor unaffected. The beam waist (340 μm in diameter) is located between the two prongs of the QTF, which has a gap of 800 μm, a resonant frequency of 7.2 kHz and a Q-factor of ~8000 (gas pressure 760 Torr) [15]. Photoacoustic gas sensors using QTF as an acoustic transducer have been previously developed for detecting many different gas species [15–17]. The optical resonator, the acoustic resonator and the QTF are all enclosed inside a chamber (PAS cell in Fig. 2). A high-speed lithium niobate optical switch (NanoSpeed, Agiltron) is used to chop the laser beam at the same frequency as the resonant frequency of the QTF. The piezoelectric current from the QTF is collected and amplified by a trans-impedance amplifier. Finally, a lock-in amplifier (MFLI 5 MHz, Zurich Instruments) with a detection bandwidth of 1 Hz (integration time 80 ms, filter roll-off 18 dB/oct) is used to demodulate the first harmonic signal (1f) at the sensor output. To retrieve a complete spectrum, the optical cavity length is tuned by a PZT attached to one cavity mirror via the function generation.

4. Double standing wave enhancement

To evaluate the enhancement effects contributed by the integrated acoustic and optical resonators, the PAS-1f signal of the C_2H_2 line at 1531.59 nm is measured under three different configurations. Fig. 3 compares the typical PAS-1f signal measured using a bare QTF (2% C_2H_2), a QTF with the mere acoustic resonator (0.1% C_2H_2), and a QTF with the complete opto-acoustic resonator (1 ppm C_2H_2). Note that different C_2H_2 concentrations are used for these three configurations because of their quite different sensitivities. All the experiments are performed at the same incident laser power of 12 mW, lock-in detection

Fig. 1. Working principle of doubly resonant PAS. ASW: acoustic standing wave; OSW: optical standing wave; QTF: quartz tuning fork. The amplitude of the OSW is modulated at the resonant frequency of the QTF. The geometry of the acoustic resonator is designed according to the acoustic frequency.
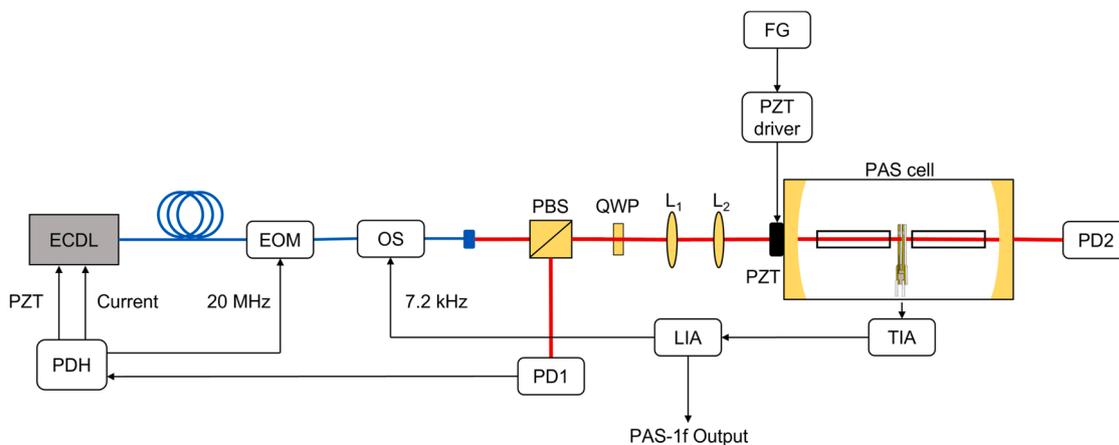
Fig. 2. Schematic of the photoacoustic sensor with opto-acoustic resonance. ECDL, external cavity diode laser; EOM, electro-optic modulator; OS, optical switch; PBS, polarization beam splitter; QWP, quarter-wave plate; PD, photodetector; PZT, piezo transducer; FG, function generator; PDH, phase demodulator and laser servo (PDD110/mFALC110, TOPTICA Photonics); TIA, trans-impedance amplifier; LIA, lock-in amplifier. The opto-acoustic resonance element inside the PAS cell has the same configuration as that shown in Fig. 1.
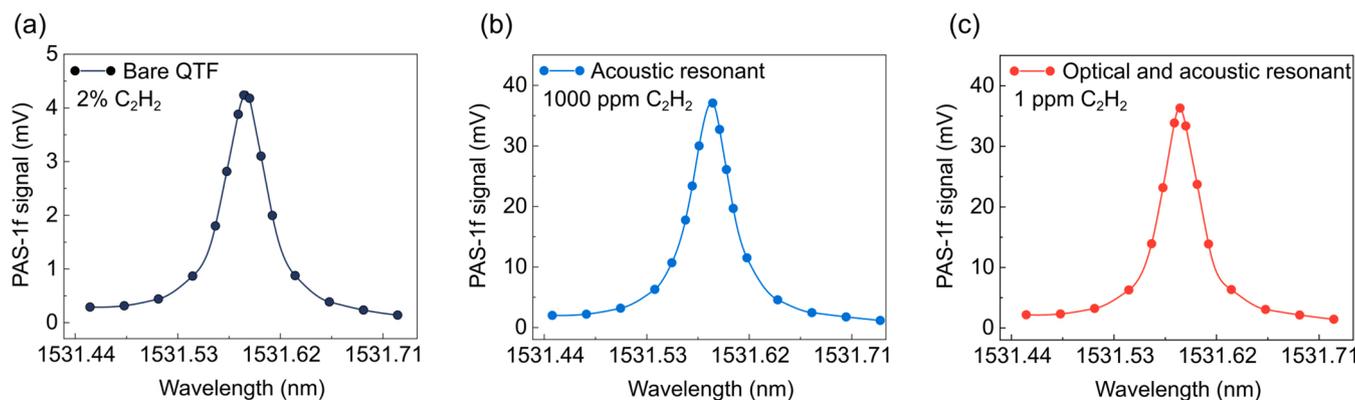
Fig. 3. PAS-1f signal measured by three different configurations: (a) bare QTF, (b) QTF with acoustic resonator, and (c) QTF with acoustic and optical resonators. The amplitude of the single-pass PAS signal measured for 2% C_2H_2/N_2 using the bare QTF is about 4.24 mV. Benefitting from the double standing wave enhancement, the sensor has a response of 36 mV to 1 ppm C_2H_2. An enhancement factor of up to five orders of magnitude for the PAS signal is achieved.

bandwidth of 1 Hz, and gas pressure of 760 Torr. After normalization by the gas concentration, a comparison of Fig. 3(a) and (b) shows that the PAS-1f signal is enhanced by 175 times. However, with the high concentration C_2H_2 used in the bare QTF measurement, we must consider power attenuation for the incident power before reaching the QTF. With a power attenuation of 17.3%, the enhancement factor of acoustic resonator is evaluated as 144. Besides, the optical resonator provides another enhancement factor of 980, as emerging from a comparison of Fig. 3(b) and (c). Hence, the combined opto-acoustic amplification provides an overall enhancement of the PAS signal by a factor of 10^5 via the double standing wave effect.

5. Ultrasensitive gas detection

Fig. 4 shows the results of C_2H_2 detection with doubly resonant PAS. The measurement of PAS-1f signal is performed with an incident optical power of 12 mW at 760 Torr for different C_2H_2 concentrations (1 ppm, 100 ppb, 10 ppb and 1 ppb in nitrogen balance) and high-purity nitrogen (99.999% purity) when the laser wavelength is tuned from 1531.32 nm to 1531.75 nm, as shown from Fig. 4(a) to (e). Note that the background signal is caused by unwanted absorption at the optical windows and resonator mirrors [31]. This background signal is not subtracted from the PAS-1f signal shown in Fig. 4. Interestingly, due to the excellent signal-to-noise ratio, a neighboring water line with quite low intensity of

2.896×10^{-24} cm^{-1}/(molec·cm^{-2}) near 1531.37 nm is detected, as shown in Fig. 4. This is probably due to residual water in the gas chamber after the desiccation process (Appendix C). Our hypothesis is confirmed by repeating the measurement of pure nitrogen (water vapor < 0.3 ppm) shown in Fig. 4(d). To reduce the measurement error, a multi-spectral fitting method, with prior knowledge of infrared spectra from the HITRAN database, is implemented [32,33]. Hence, the background signal is automatically eliminated during the fitting procedure.

The relationship between the PAS-1f signal and incident laser power is also investigated. Fig. 4(e) compares the PAS-1f signal at 1 ppb C_2H_2 under two different incident power levels (12 mW and 300 mW). The peak value of the PAS-1f signal is increased by a factor of about 22.5 when the incident laser power is increased from 12 mW to 300 mW (a factor of 25). The slight deviation of the enhancement factor between laser power and PAS signal is caused by the variation of the optical coupling efficiency. By repeating the measurement at 100 ppb C_2H_2, Fig. 4(f) shows the variation of the PAS-1f amplitude with the incident optical power. The sensor signal (red circles) increases almost linearly (0.25 mV/mW) with the incident power. In contrast, the noise level (black rectangles) remains almost unchanged over the entire power range, as shown in Fig. 4(f) (1-σ standard deviation of N_2 over 120 s). This makes our set-up very promising to further enhance the minimum detection limit by simply increasing the incident laser power.
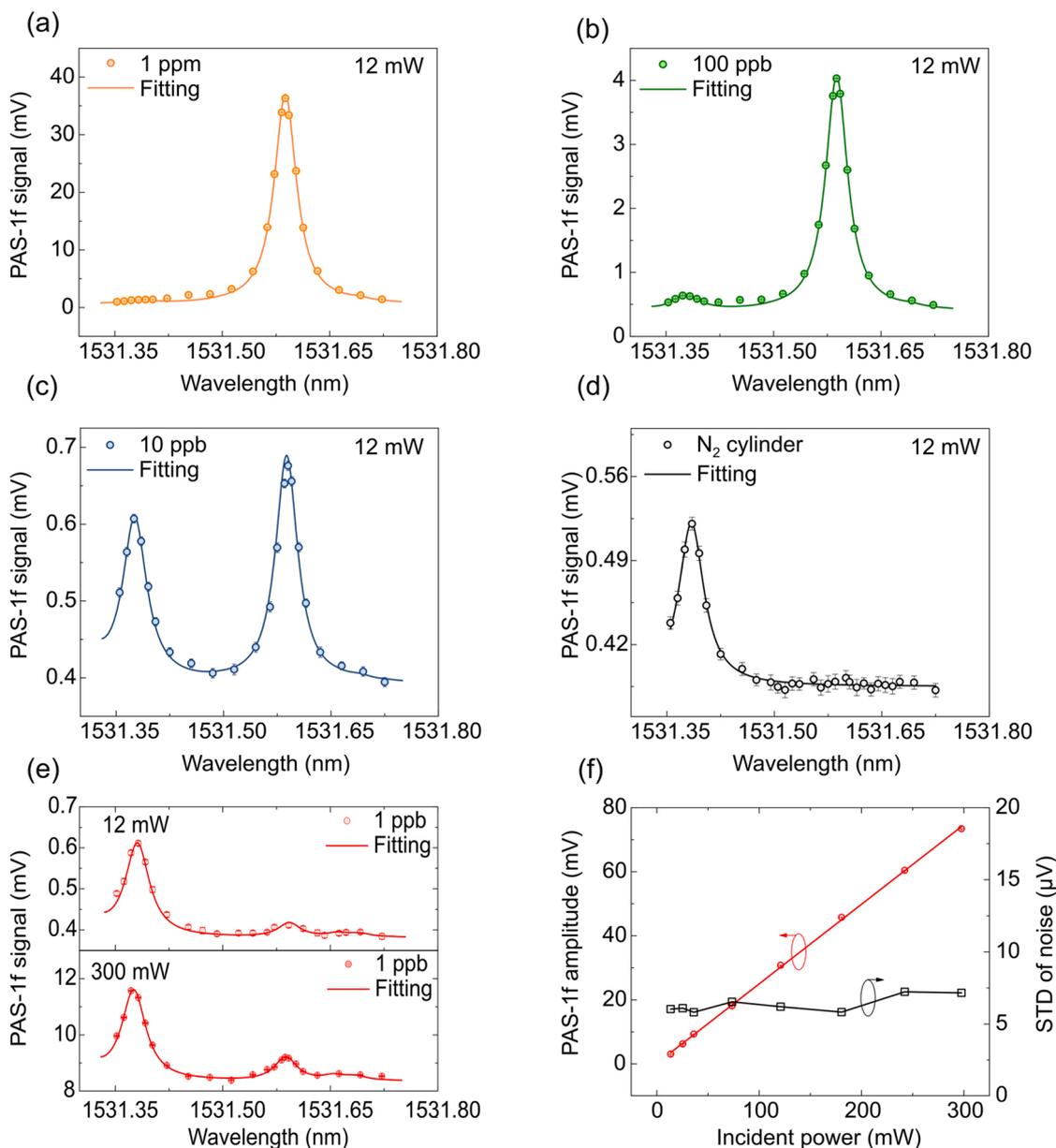
Fig. 4. Results of C_2H_2 detection with doubly resonant PAS. Representative PAS-1f signal of C_2H_2/N_2 mixtures and N_2 balance gas: (a) 1 ppm, (b) 100 ppb, (c) 10 ppb and (d) N_2 cylinder. The target C_2H_2 peak is observed at 1531.59 nm, whereas another H_2O line is also evident at 1531.37 nm. (e) Representative PAS-1f signal of 1 ppb C_2H_2 measured at two different incident optical power levels: 12 mW (top panel) and 300 mW (bottom panel). (f) PAS-1f amplitude for 100 ppb C_2H_2 and 1-σ standard deviation (STD) of the noise (a measurement of nitrogen over 120 s) versus incident power. The PAS-1f amplitudes of 100 ppb C_2H_2 at different incident power levels are inferred from the fitting results. All these measurements are performed at 760 Torr and a detection bandwidth of 1 Hz. The error bars (1-σ STD) are calculated from the raw data taken in a time interval of 120 s.

5.1. Dynamic range and detection limit

The linear response of the sensor is tested at the pressure of 760 Torr by filling the gas chamber with different C_2H_2/N_2 mixtures. Fig. 5(a) shows the background-subtracted PAS-1f amplitude as a function of C_2H_2 concentration, varying in a 1 ppb–500 ppm interval. The sensor shows a very good linear response with a slope of 36.4 μV/ppb and an R-square value of 0.99 from 1 ppb to 50 ppm. Considering the incident optical power of 12 mW, the normalized linear response coefficient of the sensor is 3 μV/(mW·ppb). Due to the linear relationship between incident optical power and PAS-1f amplitude verified in Fig. 4(f), the response coefficient remains unchanged at 300 mW. However, the sensor deviates from the linear response at higher C_2H_2 concentrations due to the apparent degradation of finesse of the optical resonator. With

an incident optical power of 300 mW, the sensor precision has also been evaluated by measuring each concentration for 120 s; here the relative precision is defined by the ratio of the standard deviation (1-σ) to the average. The sensor shows a precision of 0.1–1.1% for the C_2H_2 concentration range from 10 ppb to 1 ppb. The relative precision remains below 0.1% for gas concentrations over 10 ppb.

To evaluate the long-term stability and the minimum detection limit, the Allan–Werle deviation analysis is conducted by measuring nitrogen with the results shown in Fig. 5(b). The noise equivalent concentration (NEC) is determined to be 5.1 ppt (unity for signal-to-noise ratio) at an averaging time of 1 s. At an incident optical power of 300 mW and a detection bandwidth of 1 Hz, we obtain a NNEA coefficient of 1.7×10^{-12} W·cm^{-1}·Hz$^{-1/2}$ (Appendix D). The NEC can be improved to 0.5 ppt at a longer averaging time of 300 s, leading to a NEA coefficient
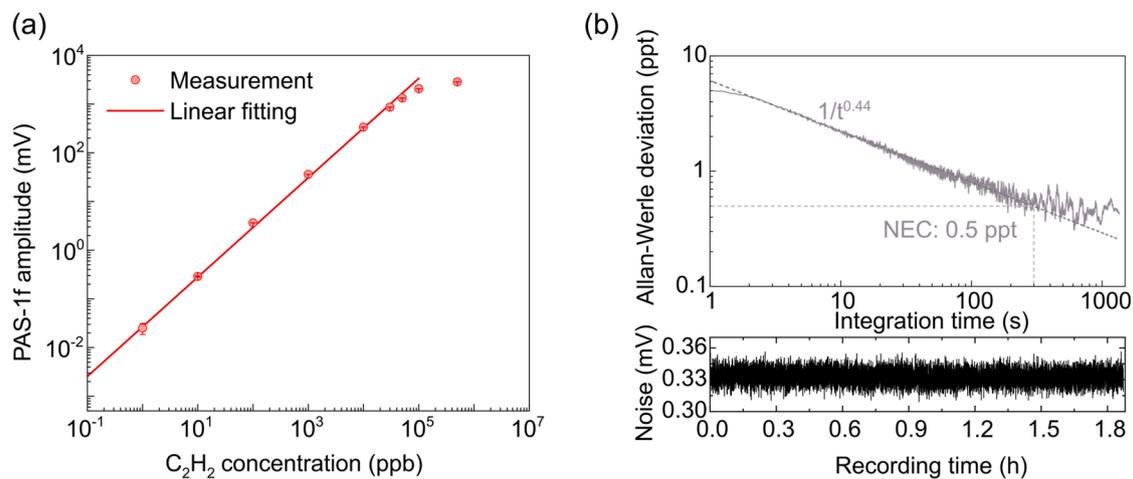
Fig. 5. Evaluation of the sensor performance. (a) Background-subtracted PAS-1f amplitude as a function of gas concentration for an incident optical power of 12 mW. Error bars show the 1-σ standard deviation from 120 s measurements. (b) The Allan–Werle deviation analysis. The laser wavelength is tuned to the peak of the C_2H_2 absorption line, with the chamber filled with nitrogen. The dashed line in the top panel represents the $1/t^{0.44}$ slope. The bottom panel depicts the raw data of noise measured for nearly 2 h. The detection bandwidth is the same as the signal measurement.

of 5.7×10^{-13} cm^{-1}. As a result, the proposed photoacoustic gas sensor achieves a dynamic range of 1.0×10^8 (Appendix E). The dynamic stability of the sensor is evaluated by operating the gas sensor when continuously filling C_2H_2/N_2 gas samples into the gas chamber (see Supplementary Note 3).

6. Discussion and conclusions

The key performance parameters (e.g., dynamic range, NEC, and NEA) of some state-of-the-art gas sensors are summarized in Table 1. The photoacoustic gas sensor developed in this work shows a dynamic range and NEA, superior to the state-of-the-art photoacoustic sensors using different types of laser sources and acoustic transducers. Most remarkably, the current dynamic range is three orders of magnitude wider than the state-of-the-art (10^5) [23], and the current NEA is two orders of magnitude better than the state-of-the-art (10^{-11} cm^{-1}) [22]. Compared to other state-of-the-art gas sensors based on various spectroscopic methods such as NICE-OHMS, SCAR, CRDS and off-axis integrated cavity output spectroscopy (OA-ICOS) [6,9,34,35], NICE-OHMS and CRDS exhibit 57 times and 4 times better sensitivities, respectively. But our sensor shows evident merits of size (5–8 times shorter cavity) and dynamic range (2–3 orders wider). It is worth mentioning that, among

the state-of-the-art PAS studies, the cantilever with an interferometer readout has been proven to be the most sensitive acoustic transducer [22].

In summary, we have developed a photoacoustic gas sensor using an integrated optical-acoustic resonator. Taking advantage of a double standing wave enhancement, the photoacoustic signal has been improved by five orders of magnitude compared to a bare QTF, thus providing ultrasensitive gas detection with low-power semiconductor lasers. The moderate cavity finesse maintains the high coupling efficiency of the incident laser and enables a wide dynamic range by using a short optical resonator. As a result, we have demonstrated a photoacoustic sensor for C_2H_2 (balanced in nitrogen) with a NEC of 0.5 ppt, a NEA of 5.7×10^{-13} cm^{-1}, and a dynamic range of eight orders of magnitude. Although the demonstration is performed in the near-infrared region, the concept can be extended to the mid-infrared range to take advantage of the much stronger fundamental absorption bands. One may expect the possible challenges of obtaining high-quality mid-infrared laser beams and suitable acoustic resonators.

Declaration of Competing Interest

The authors declare no conflicts of interest.

Table 1
Main parameters of state-of-the-art laser-based gas sensors.

Gas	Method		λ (μm)	L (mm)	D	NEC (ppt)	NEA (cm^{-1})	t (s)	P (Torr)
NO$_2$	PAS [23]	PAS	0.45	NA	1×10^5	54	2.3×10^{-10}	1	640
SF$_6$	QEPAS [24]		10.5	NA	3×10^3	50	6.1×10^{-9}	1	75
CO$_2$	I-QEPAS [17]		4.33	174	3×10^3	300	1.4×10^{-8}	20	38
C$_2$H$_2$	CECEPAS [22]		1.53	147	7×10^3	24	2.4×10^{-11}	100	150
C$_2$H$_2$	CE-PAS [21]		1.53	130	1×10^4	300	1.9×10^{-10}	300	50
HF	CEPAS [13]		2.47	NA	4×10^4	0.65	1.3×10^{-10}	1920	150
SF$_6$	α-BiB$_3$O$_6$-PAS [14]		10.6	NA	1×10^5	0.75	8.1×10^{-11}	100	760
C$_2$H$_2$	**This work**		**1.53**	**60**	**1×10^8**	**0.5**	**5.7×10^{-13}**	**300**	**760**
^{14}CO$_2$	SCAR [6]	CEAS	4.5	1000	NS	0.005	1.1×10^{-12}	7200	9.12
CO$_2$	CRDS [34]		1.6	330	7×10^5	40,000	1.4×10^{-13}	4	0.075
C$_2$HD	NICE-OHMS [9]		1.06	469	NS	NS	1×10^{-14}	1	0.0018
CO	OA-ICOS [35]		1.57	1100	NS	1000	1.9×10^{-12}	1	197

λ: laser wavelength. L: cavity length. D: dynamic range. t: averaging time. P: pressure. CEAS: cavity-enhanced absorption spectroscopy. NA: not applicable. NS: not stated.

Note that the dynamic range values are calculated using the same definition in the Appendix E. The two PAS sensors that can achieve sub-ppt sensitivity use mid-infrared lasers [13,14]. The NEAs with different averaging times are listed here because these sensors have different stabilities. A sensor may have a sensitivity improvement by averaging if it is stable enough with white noise dominant. The averaging time is not normalized here as it cannot reflect the ultimate performance of sensors.

Appendix A. Selection of finesse for the optical resonator

The finesse of the optical resonator needs to be properly selected in this work. First, the selection of a higher finesse theoretically provides a larger power enhancement factor. However, the linewidth of the cavity mode decreases with the increased finesse, making it more challenging to achieve a high coupling efficiency of the laser into the optical resonator [36]. Second, the dynamic range of the sensor is affected by the finesse. The finesse is determined by the round-trip loss inside the optical resonator which includes the mirror transmission and absorption, gas absorption, and loss induced by the acoustic module [36]. The finesse increases with the larger reflectivity of cavity mirrors, but it decreases apparently when the loss induced by gas absorption becomes comparable [17,21]. Hence, the physical length of the optical resonator should be selected as short as possible to minimize the gas-absorption loss inside the cavity. It is important to prevent the intracavity laser beam from being partly blocked by the QTF and acoustic resonator, which may in turn increase the noise and decrease the optical enhancement factor. Hence, there is a tradeoff between the optimal inner diameter of the acoustic resonator and the length of the optical resonator. Besides, the QTF and acoustic resonator also set a lower limit of the length of the optical resonator.

In this work, a moderate finesse of about 4000 (mirror reflectivity, 99.923%) and a physical length of 60 mm is used.

Appendix B. Calibration of intracavity laser power

According to the main text, the optical resonator enhances the photoacoustic signal by a factor of 980. Considering the 84% coupling efficiency, the intracavity power enhancement factor is 1166, which is slightly lower than the theoretical buildup factor of 1300. This is probably due to the extra cavity loss caused by the QTF. As the empty cavity has a finesse of 4078, an additional loss of 0.017% can deteriorate the buildup factor from 1300 to 1166. When the incident power is adjusted from 12 mW to 300 mW, there is an extra 10% degradation of coupling efficiency. Hence, the maximum of the intracavity power is determined to be 264 W, by the product of the incident laser power (300 mW), the power enhancement factor of the empty cavity (1166) and the coupling efficiency (84%×(1–10%)= 75.6%).

Appendix C. Gas chamber dehumidification

To mitigate the interference of the residual water molecules, the gas chamber is heated to 60 ℃ and purged continuously by dry nitrogen for several hours. To protect the QTF which is quite close to the acoustic resonator, the heating temperature is controlled not quite high. It is possible to have some residual water inside the chamber.

Appendix D. NNEA calculation

The NNEA coefficient can be calculated by the following equation:

$$NNEA = \frac{\alpha_{\min} \times W_{in}}{\sqrt{BW}}$$

where $\alpha_{\min}$ is the noise equivalent absorption (NEA), W_{in} is the incident power and BW is the detection bandwidth. With the NEC of 5.1 ppt in Fig. 5(b), NEA can be easily obtained by referencing to the HITRAN database [32]. The incident power is 300 mW. Together with the detection bandwidth of 1 Hz, the NNEA of 1.7×10^{-12} W·cm^{-1}·Hz$^{-1/2}$ can be calculated.

Appendix E. Dynamic range definition

The dynamic range of a gas sensor is defined as the maximum concentration that is in the linear fitting range divided by the NEC [37–39]. In this work, the maximum concentration in the linear fitting range is 50 ppm and the NEC is 0.5 ppt, leading to a dynamic range of eight orders of magnitude.

Appendix F. Supplementary data

See the supplementary material for detailed descriptions of characterization of mirror reflectivity, evaluation of optical coupling efficiency and dynamic stability of the sensor.

Appendix A. Supporting information

Supplementary data associated with this article can be found in the online version at doi:10.1016/j.pacs.2022.100387.

References

[1] L.B. Kreuzer, C.K.N. Patel, Nitric oxide air pollution: detection by optoacoustic spectroscopy, Science 173 (3991) (1971) 45–47.

[2] G.B. Rieker, F.R. Giorgetta, W.C. Swann, J. Kofler, A.M. Zolot, L.C. Sinclair, E. Baumann, C. Cromer, G. Petron, C. Sweeney, P.P. Tans, I. Coddington, N. R. Newbury, Frequency-comb-based remote sensing of greenhouse gases over kilometer air paths, Optica 1 (5) (2014) 290–298.

[3] E.A. Kort, S.C. Wofsy, B.C. Daube, M. Diao, J.W. Elkins, R.S. Gao, E.J. Hintsa, D. F. Hurst, R. Jimenez, F.L. Moore, J.R. Spackman, M.A. Zondlo, Atmospheric observations of Arctic Ocean methane emissions up to 82° north, Nat. Geosci. 5 (5) (2012) 318–321.

[4] B.F. Thornton, J. Prytherch, K. Andersson, I.M. Brooks, D. Salisbury, M. Tjernström, P.M. Crill, Shipborne eddy covariance observations of methane fluxes constrain Arctic sea emissions, Sci. Adv. 6 (5) (2020) eaay7934.

[5] R. Adato, H. Altug, In-situ ultra-sensitive infrared absorption spectroscopy of biomolecule interactions in real time with plasmonic nanoantennas, Nat. Commun. 4 (2013) 2154.

[6] I. Galli, S. Bartalini, R. Ballerini, M. Barucci, P. Cancio, M.D. Pas, G. Giusfredi, D. Mazzotti, N. Akikusa, P. De Natale, Spectroscopic detection of radiocarbon dioxide at parts-per-quadrillion sensitivity, Optica 3 (4) (2016) 385–388.

[7] C. Wang, P. Sahay, Breath analysis using laser spectroscopic techniques: breath biomarkers, spectral fingerprints, and detection limits, Sensors 9 (10) (2009) 8230–8262.

[8] Q. Liang, Y.C. Chan, P.B. Changala, D.J. Nesbitt, J. Ye, J. Toscano, Ultrasensitive multispecies spectroscopic breath analysis for real-time health monitoring and diagnostics, Proc. Natl. Acad. Sci. USA 118 (40) (2021), e2105063118.

[9] J. Ye, L.S. Ma, J.L. Hall, Ultrasensitive detections in atomic and molecular physics: demonstration in molecular overtone spectroscopy, J. Opt. Soc. Am. B 15 (1) (1998) 6–15.

[10] M.G. Delli Santi, S. Bartalini, P. Cancio, I. Galli, G. Giusfredi, C. Haraldsson, D. Mazzotti, A. Pesonen, P. De Natale, Biogenic fraction determination in fuel blends by laser-based $^{14}CO_2$ detection, Adv. Photonics Res. 2 (3) (2021), 2000069.

[11] A. Foltynowicz, F.M. Schmidt, W. Ma, O. Axner, Noise-immune cavity-enhanced optical heterodyne molecular spectroscopy: current status and future potential, Appl. Phys. B 92 (3) (2008) 313.

[12] S. Manakasetharn, A. Takahashi, T. Kawamoto, K. Noda, Y. Sugiyama, T. Nakamura, Highly sensitive and exceptionally wide dynamic range detection of ammonia gas by indium hexacyanoferrate nanoparticles using FTIR spectroscopy, Anal. Chem. 90 (7) (2018) 4856–4862.

[13] T. Tomberg, M. Vainio, T. Hieta, L. Halonen, Sub-parts-per-trillion level sensitivity in trace gas detection by cantilever-enhanced photo-acoustic spectroscopy, Sci. Rep. 8 (2018) 1848.

[14] L. Xiong, W. Bai, F. Chen, X. Zhao, F. Yu, G.J. Diebold, Photoacoustic trace detection of gases at the parts-per-quadrillion level with a moving optical grating, Proc. Natl. Acad. Sci. USA 114 (28) (2017) 7246–7249.

[15] H. Wu, A. Sampaolo, L. Dong, P. Patimisco, X. Liu, H. Zheng, X. Yin, W. Ma, L. Zhang, W. Yin, V. Spagnolo, S. Jia, F.K. Tittel, Quartz enhanced photoacoustic H_2S gas sensor based on a fiber-amplifier source and a custom tuning fork with large prong spacing, Appl. Phys. Lett. 107 (11) (2015), 111104.

[16] H. Zheng, L. Dong, A. Sampaolo, H. Wu, P. Patimisco, X. Yin, W. Ma, L. Zhang, W. Yin, V. Spagnolo, S. Jia, F.K. Tittel, Single-tube on-beam quartz-enhanced photoacoustic spectroscopy, Opt. Lett. 41 (5) (2016) 978–981.

[17] S. Borri, P. Patimisco, I. Galli, D. Mazzotti, G. Giusfredi, N. Akikusa, M. Yamanishi, G. Scamarcio, P. De Natale, V. Spagnolo, Intracavity quartz-enhanced photoacoustic sensor, Appl. Phys. Lett. 104 (9) (2014), 091114.

[18] J. Wojtas, A. Gluszek, A. Hudzikowski, F.K. Tittel, Mid-infrared trace gas sensor technology based on intracavity quartz-enhanced photoacoustic spectroscopy, Sensors 17 (3) (2017) 513.

[19] M. Hippler, C. Mohr, K.A. Keen, E.D. McNaghten, Cavity-enhanced resonant photoacoustic spectroscopy with optical feedback cw diode lasers: a novel technique for ultratrace gas analysis and high-resolution spectroscopy, J. Chem. Phys. 133 (4) (2010), 044308.

[20] A. Kachanov, S. Koulikov, F.K. Tittel, Cavity-enhanced optical feedback-assisted photo-acoustic spectroscopy with a 10.4 µm external cavity quantum cascade laser, Appl. Phys. B 110 (2013) 47–56.

[21] Z. Wang, Q. Wang, W. Zhang, H. Wei, Y. Li, W. Ren, Ultrasensitive photoacoustic detection in a high-finesse cavity with Pound–Drever–Hall locking, Opt. Lett. 44 (8) (2019) 1924–1927.

[22] T. Tomberg, T. Hieta, M. Vainio, L. Halonen, Cavity-enhanced cantilever-enhanced photo-acoustic spectroscopy, Analyst 144 (7) (2019) 2291–2296.

[23] X. Yin, L. Dong, H. Wu, H. Zheng, W. Ma, L. Zhang, W. Yin, S. Jia, F.K. Tittel, Sub-ppb nitrogen dioxide detection with a large linear dynamic range by use of a differential photoacoustic cell and a 3.5 W blue multimode diode laser, Sens. Actuators B Chem. 247 (2017) 329–335.

[24] V. Spagnolo, P. Patimisco, S. Borri, G. Scamarcio, B.E. Bernacki, J. Kriesel, Part-per-trillion level SF_6 detection using a quartz enhanced photoacoustic spectroscopy-based sensor with single-mode fiber-coupled quantum cascade laser excitation, Opt. Lett. 37 (21) (2012) 4461–4463.

[25] J. Hayden, M. Giglio, A. Sampaolo, V. Spagnolo, B. Lendl, Mid-Infrared intracavity quartz-enhanced photoacoustic spectroscopy with pptv–level sensitivity using a T-shaped custom tuning fork, Photoacoustics 25 (2022), 100330.

[26] A.J. Friss, C.M. Limbach, A.P. Yalin, Cavity-enhanced rotational Raman scattering in gases using a 20 mW near-infrared fiber laser, Opt. Lett. 41 (14) (2016) 3193–3196.

[27] L. Dong, A.A. Kosterev, D. Thomazy, F.K. Tittel, QEPAS spectrophones: design, optimization, and performance, Appl. Phys. B 100 (3) (2010) 627–635.

[28] S.D. Russo, A. Sampaolo, P. Patimisco, G. Menduni, M. Giglio, C. Hoelzl, V.M. N. Passaro, H. Wu, L. Dong, V. Spagnolo, Quartz-enhanced photoacoustic spectroscopy exploiting low-frequency tuning forks as a tool to measure the vibrational relaxation rate in gas species, Photoacoustics 21 (2021), 100227.

[29] A. Miklós, P. Hess, Z. Bozóki, Application of acoustic resonators in photoacoustic trace gas analysis and metrology, Rev. Sci. Instrum. 72 (4) (2001) 1937–1955.

[30] R.W.P. Drever, J.L. Hall, F.V. Kowalski, J. Hough, G.M. Ford, A.J. Munley, H. Ward, Laser phase and frequency stabilization using an optical resonator, Appl. Phys. B 31 (2) (1983) 97–105.

[31] L. Liu, H. Huan, X. Zhang, L. Zhang, X. Shao, A. Mandelis, L. Dong, Laser induced thermoelastic contributions from windows to signal background in a photoacoustic cell, Photoacoustics 22 (2021), 100257.

[32] I.E. Gordon, L.S. Rothman, C. Hill, R.V. Kochanov, Y. Tan, P.F. Bernath, M. Birk, V. Boudon, A. Campargue, K.V. Chance, B.J. Drouin, J.M. Flaud, R.R. Gamache, J. T. Hodges, D. Jacquemart, V.I. Perevalov, A. Perrin, K.P. Shine, M.-A.H. Smith, J. Tennyson, G.C. Toon, H. Tran, V.G. Tyuterev, A. Barbe, A.G. Csaszar, V.M. Devi, T. Furtenbacher, J.J. Harrison, J.-M. Hartmann, A. Jolly, T.J. Johnson, T. Karman, I. Kleiner, A.A. Kyuberis, J. Loos, O.M. Lyulin, S.T. Massie, S.N. Mikhailenko, N. Moazzen-Ahmadi, H.S.P. Müller, O.V. Naumenko, A.V. Nikitin, O.L. Polyansky, M. Rey, M. Rotger, S.W. Sharpe, K. Sung, E. Starikova, S.A. Tashkun, J. Vander Auwera, G. Wagner, J. Wilzewski, P. Wcisło, S. Yu, E.J. Zak, The HITRAN2016 molecular spectroscopic database, J. Quant. Spectrosc. Radiat. Transf. 203 (2017) 3–69.

[33] C.S. Goldenstein, V.A. Miller, R.M. Spearrin, C.L. Strand, SpectraPlot. com: Integrated spectroscopic modeling of atomic and molecular gases, J. Quant. Spectrosc. Radiat. Transf. 200 (2017) 249–257.

[34] J. Burkart, D. Romanini, S. Kassi, Optical feedback frequency stabilized cavity ring-down spectroscopy, Opt. Lett. 39 (16) (2014) 4695–4698.

[35] G.S. Engel, W.S. Drisdell, F.N. Keutsch, E.J. Moyer, J.G. Anderson, Ultrasensitive near-infrared integrated cavity output spectroscopy technique for detection of CO at 1.57 µm: new sensitivity limits for absorption measurements in passive optical cavities, Appl. Opt. 45 (36) (2006) 9221–9229.

[36] D. Romanini, I. Ventrillard, G. Méjean, J. Morville, E. Kerstel, Introduction to cavity enhanced absorption spectroscopy, Cavity-Enhanced Spectroscopy and Sensing, Springer, Berlin, Heidelberg, 2014, pp. 1–60.

[37] W. Jin, Y. Cao, F. Yang, H.L. Ho, Ultra-sensitive all-fibre photothermal spectroscopy with large dynamic range, Nat. Commun. 6 (2015) 7767.

[38] P. Zhao, Y. Zhao, H. Bao, H.L. Ho, W. Jin, S. Fan, S. Gao, Y. Wang, P. Wang, Mode-phase-difference photothermal spectroscopy for gas detection with an anti-resonant hollow-core optical fiber, Nat. Commun. 11 (2020) 847.

[39] X. Lou, Y. Feng, S. Yang, Y. Dong, Ultra-wide-dynamic-range gas sensing by optical pathlength multiplexed absorption spectroscopy, Photonics Res. 9 (2) (2021) 193.

Zhen Wang is currently a postdoc fellow at the National Institute of Optics (CNR-INO) in Italy. He received his Ph.D. degree from the Chinese University of Hong Kong. After that, he worked as a research associate in the Chinese University of Hong Kong and a visiting scholar at Changchun Institute of Optics, Fine Mechanics and Physics, Chinese Academy of Science. His research interests are trace gas sensing and laser spectroscopy.

Qiang Wang is currently a professor in the State Key Laboratory of Applied Optics at Changchun Institute of Optics, Fine Mechanics and Physics, Chinese Academy of Sciences. He received his B.S. degree in Electronic Science and Technology in 2011 and Ph.D. degree in Optical Engineering in 2016 from Shandong University. After his graduate study, he worked as a postdoctoral fellow at the Chinese University of Hong Kong and Max Planck Institute of Quantum Optics successively. His recent research interests are laser spectroscopy, optical sensing, and engineering application of trace gas analysis in the atmosphere, deep sea, and public health.

Hui Zhang received his BEng degree from Ocean University of China in 2019. He is currently a PhD student at Changchun Institute of Optics, Fine Mechanics and Physics, Chinese Academy of Sciences. His research project is on fiber sensing and laser spectroscopy.

Simone Borri has completed his PhD in 2007 from University of Firenze, Italy. He is researcher at CNR-National Institute of Optics since 2010. He worked as researcher for LENS, the European Laboratory for Nonlinear Spectroscopy, and IFN, the italian Institute for Photonics and Nanotechnologies. His area of expertize includes the development of narrow-linewidth metrological-grade coherent sources and techniques for high-sensitivity and high-precision molecular spectroscopy in the mid infrared.

Iacopo Galli is currently a researcher of National Institute of Optics of the Italian National Research Council (CNR-INO). He received his Ph.D. degree in physics from University of Florence in 2009. Since 2009 he works in CNR-INO, first as post-doctoral researcher and today as researcher. In 2016 he have co-founded a spin-off of the National Research Council named ppqSense, the core business of the company is the radiocarbon detection with SCAR technique. His current research interests include nonlinear optics, high-sensitivity and high-precision infrared laser spectroscopy, gas sensing, frequency metrology, and quantum-cascade lasers characterization and stabilization.

Angelo Sampaolo obtained his Master degree in Physics in 2013 and the PhD Degree in Physics in 2017 from University of Bari. He was an associate researcher in the Laser Science Group at Rice University from 2014 to 2016 and associate researcher at Shanxi University since 2018. Since May 2017, he was a Post-Doctoral Research associate at University of Bari and starting from December 2019, he is Assistant Professor at Polytechnic of Bari. His research activity has included the study of the thermal properties of heterostructured devices via Raman spectroscopy. Most recently, his research interest has focused on the development of innovative techniques in trace gas sensing, based on Quartz-Enhanced Photoacoustic Spectroscopy and covering the full spectral range from near-IR to THz. His achieved results have been acknowledged by a cover paper in Applied Physics Letter of the July 2013 issue.

Pietro Patimisco obtained the Master degree in Physics (cum laude) in 2009 and the PhD Degree in Physics in 2013 from the University of Bari. Since 2018, he is Assistant professor at the Technical University of Bari. He was a visiting scientist in the Laser Science Group at Rice University in 2013 and 2014. Dr. Patimisco's scientific activity addressed both micro-probe optical characterization of semiconductor optoelectronic devices and optoacoustic gas sensors. Recently, his research activities included the study and applications of trace-gas sensors, such as quartz enhanced photoacoustic spectroscopy and cavity enhanced absorption spectroscopy in the mid infrared and terahertz spectral region, leading to several publications, including a cover paper in Applied Physics Letter of the July 2013 issue.

Angelo Sampaolo obtained the PhD in physics in 1994 from University of Bari. From 1997–1999, he was researcher of the National Institute of the Physics of Matter. Since 2004, he works at the Technical University of Bari, formerly as assistant and associate professor and now as full Professor of Physics. Starting from 2019, he become Vice-Rector of the technical university of Bari - Deputy to Technology Transfer. He is the director of the joint-research lab PolySense between Technical University of Bari and THORLABS GmbH, fellow member of SPIE and senior member of OSA. His research interests include optoacoustic gas sensing and spectroscopic techniques for realtime monitoring. His research activity is documented by more than 220 publications and 3 filed patents. He has given more than 50 invited presentations at international conferences and workshops.

Paolo De Natale is research director at the National Institute of Optics-INO (Italian CNR) and member of the Directive Council of LENS, Firenze, Italy. In the years 2007–2021 was director of the National Institute of Optics of the Italian National Research Council (INO-CNR, former INOA). He is the Italian representative in the Quantum Community Network (QCN) Board of the EU Flagship on Quantum Technologies and in the Optronics CapTech of the European Defense Agency-EDA. Scientific interests include photonics, atomic and molecular physics, nonlinear optics and quantum technologies. He is author of more than 360 publications, owns 9 patents and is a co-founder of two former CNR spin-off companies, ppqSense srl and QTI srl. He is Fellow of IEEE (since 2011) and OSA (since 2015).

Wei Ren received the B.S. degree in Mechanical Engineering and M.S. degree in Optical Engineering from Tsinghua University in 2006 and 2008, respectively. He received the Ph.D. degree in Mechanical Engineering from Stanford University in 2013. He was awarded the Robert A. Welch Foundation postdoctoral fellowship to work in the Department of Electrical and Computer Engineering at Rice University in 2013–14. Dr. Ren is now an associate professor in the Department of Mechanical and Automation Engineering at the Chinese University of Hong Kong. His research to date has resulted in more than 70 peer-reviewed journal publications in laser spectroscopy, optical sensing, and chemical kinetics. He is currently the co-editor of Springer journal Applied Physics B. Prof. Ren is the senior member of OSA, and member of SPIE and the Combustion Institute.